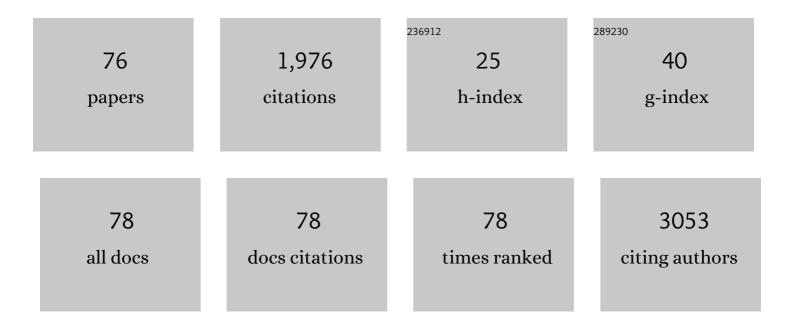
## Yikai Xu

## List of Publications by Year in descending order

Source: https://exaly.com/author-pdf/7078146/publications.pdf Version: 2024-02-01



Υικαι Χι

#	Article	IF	CITATIONS
1	A fully automatic artificial intelligence–based CT image analysis system for accurate detection, diagnosis, and quantitative severity evaluation of pulmonary tuberculosis. European Radiology, 2022, 32, 2188-2199.	4.5	30
2	Evaluation of microvascular invasion of hepatocellular carcinoma using whole-lesion histogram analysis with the stretched-exponential diffusion model. British Journal of Radiology, 2022, 95, 20210631.	2.2	3
3	Functionalized Au@Cu-Sb-S Nanoparticles for Spectral CT/Photoacoustic Imaging-Guided Synergetic Photo-Radiotherapy in Breast Cancer. International Journal of Nanomedicine, 2022, Volume 17, 395-407.	6.7	6
4	A tumor microenvironment dual responsive contrast agent for contrary contrast-magnetic resonance imaging and specific chemotherapy of tumors. Nanoscale Horizons, 2022, 7, 403-413.	8.0	9
5	Predicting peritoneal recurrence and disease-free survival from CT images in gastric cancer with multitask deep learning: a retrospective study. The Lancet Digital Health, 2022, 4, e340-e350.	12.3	45
6	Rapid synthesis of †yolk-shell'-like nanosystem for MR molecular and chemo-radio sensitization. Journal of Controlled Release, 2022, 347, 55-67.	9.9	8
7	Intestinal fibrosis classification in patients with Crohn's disease using CT enterography–based deep learning: comparisons with radiomics and radiologists. European Radiology, 2022, 32, 8692-8705.	4.5	30
8	Development and Validation of a Deep Learning CT Signature to Predict Survival and Chemotherapy Benefit in Gastric Cancer. Annals of Surgery, 2021, 274, e1153-e1161.	4.2	99
9	Recommendations for coronavirus disease 2019 (COVID-19) prevention and infection control in the radiology department: Chinese experience. Clinical Imaging, 2021, 69, 33-36.	1.5	11
10	Cycle-Consistent Generative Adversarial Network: Effect on Radiation Dose Reduction and Image Quality Improvement in Ultralow-Dose CT for Evaluation of Pulmonary Tuberculosis. Korean Journal of Radiology, 2021, 22, 983.	3.4	9
11	Noninvasive Prediction of Occult Peritoneal Metastasis in Gastric Cancer Using Deep Learning. JAMA Network Open, 2021, 4, e2032269.	5.9	58
12	Noninvasive Assessment of <scp>O(6)â€Methylguanineâ€DNA Methyltransferase</scp> Promoter Methylation Status in World Health Organization Grade <scp>II–IV</scp> Glioma Using Histogram Analysis of <scp>Inflowâ€Based Vascular‧paceâ€Occupancy</scp> Combined with Structural <scp>Magnetic Resonance</scp> Imaging. Journal of Magnetic Resonance Imaging, 2021, 54, 227-236.	3.4	4
13	The FTO m6A demethylase inhibits the invasion and migration of prostate cancer cells by regulating total m6A levels. Life Sciences, 2021, 271, 119180.	4.3	29
14	Preoperative Gadoxetic Acid-Enhanced MRI Based Nomogram Improves Prediction of Early HCC Recurrence After Ablation Therapy. Frontiers in Oncology, 2021, 11, 649682.	2.8	8
15	Radiographical assessment of tumour stroma and treatment outcomes using deep learning: a retrospective, multicohort study. The Lancet Digital Health, 2021, 3, e371-e382.	12.3	29
16	An attention-based deep learning model for predicting microvascular invasion of hepatocellular carcinoma using an intra-voxel incoherent motion model of diffusion-weighted magnetic resonance imaging. Physics in Medicine and Biology, 2021, 66, 185019.	3.0	8
17	Cross-Cultural Adaptation and Validation of the Emotional Inhibition Scale in a Chinese Cancer Sample. Frontiers in Psychology, 2021, 12, 654777.	2.1	0
18	Intelligent Pore Switch of Hollow Mesoporous Organosilica Nanoparticles for High Contrast Magnetic Resonance Imaging and Tumor-Specific Chemotherapy. Nano Letters, 2021, 21, 9551-9559.	9.1	31

#	Article	IF	CITATIONS
19	Radiomics signature based on computed tomography images for the preoperative prediction of lymph node metastasis at individual stations in gastric cancer: A multicenter study. Radiotherapy and Oncology, 2021, 165, 179-190.	0.6	9
20	A deformable model for navigated laparoscopic gastrectomy based on finite elemental method. Minimally Invasive Therapy and Allied Technologies, 2020, 29, 210-216.	1.2	1
21	Mitochondria-targeted aggregation-induced emission active near infrared fluorescent probe for real-time imaging. Spectrochimica Acta - Part A: Molecular and Biomolecular Spectroscopy, 2020, 224, 117456.	3.9	9
22	Residual convolutional neural network for predicting response of transarterial chemoembolization in hepatocellular carcinoma from CT imaging. European Radiology, 2020, 30, 413-424.	4.5	127
23	Radiomics of small renal masses on multiphasic CT: accuracy of machine learning–based classification models for the differentiation of renal cell carcinoma and angiomyolipoma without visible fat. European Radiology, 2020, 30, 1254-1263.	4.5	69
24	Differential detection of metastatic and inflammatory lymph nodes using intravoxel incoherent motion diffusion-weighted imaging. Magnetic Resonance Imaging, 2020, 65, 62-66.	1.8	2
25	Ultrasmall Superparamagnetic Iron Oxide Labeled Silk Fibroin/Hydroxyapatite Multifunctional Scaffold Loaded With Bone Marrow-Derived Mesenchymal Stem Cells for Bone Regeneration. Frontiers in Bioengineering and Biotechnology, 2020, 8, 697.	4.1	19
26	Radiomics Nomogram for Prediction of Peritoneal Metastasis in Patients With Gastric Cancer. Frontiers in Oncology, 2020, 10, 1416.	2.8	22
27	Clear cell renal cell carcinoma: the value of sex-specific abdominal visceral fat measured on CT for prediction of Fuhrman nuclear grade. European Radiology, 2020, 30, 3977-3986.	4.5	13
28	Functional connectivity changes of nucleus Accumbens Shell portion in left mesial temporal lobe epilepsy patients. Brain Imaging and Behavior, 2020, 14, 2659-2667.	2.1	5
29	Nonâ€Gaussian Diffusion Models and T 1 rho Quantification in the Assessment of Hepatic Sinusoidal Obstruction Syndrome in Rats. Journal of Magnetic Resonance Imaging, 2020, 52, 1110-1121.	3.4	2
30	Meta-analysis of the Value of Cardiac Nuclear Magnetic Resonance in the Diagnosis of Viral Myocarditis. Journal of the College of Physicians and SurgeonsPakistan: JCPSP, 2020, 30, 1326-1331.	0.4	0
31	Radiomics nomogram for predicting the malignant potential of gastrointestinal stromal tumours preoperatively. European Radiology, 2019, 29, 1074-1082.	4.5	52
32	Intravoxel incoherent motion diffusion-weighted MRI in patients with breast cancer: Correlation with tumor stroma characteristics. European Journal of Radiology, 2019, 120, 108686.	2.6	11
33	Early identification of neonatal mild hypoxic-ischemic encephalopathy by amide proton transfer magnetic resonance imaging: A pilot study. European Journal of Radiology, 2019, 119, 108620.	2.6	7
34	CT and CEST MRI bimodal imaging of the intratumoral distribution of iodinated liposomes. Quantitative Imaging in Medicine and Surgery, 2019, 9, 1579-1591.	2.0	24
35	Whole-tumor histogram analysis of apparent diffusion coefficient in differentiating intracranial solitary fibrous tumor/hemangiopericytoma from angiomatous meningioma. European Journal of Radiology, 2019, 112, 186-191.	2.6	28
36	Radiomics Signature on Computed Tomography Imaging: Association With Lymph Node Metastasis in Patients With Gastric Cancer. Frontiers in Oncology, 2019, 9, 340.	2.8	57

#	Article	IF	CITATIONS
37	Association of Glioma Grading With Inflowâ€Based Vascularâ€Spaceâ€Occupancy MRI: A Preliminary Study at 3T. Journal of Magnetic Resonance Imaging, 2019, 50, 1817-1823.	3.4	10
38	Ultralow-dose CT with knowledge-based iterative model reconstruction (IMR) in evaluation of pulmonary tuberculosis: comparison of radiation dose and image quality. European Radiology, 2019, 29, 5358-5366.	4.5	7
39	Clivopalate angle: a new diagnostic method for basilar invagination at magnetic resonance imaging. European Radiology, 2019, 29, 3450-3457.	4.5	7
40	Developed and validated a prognostic nomogram for recurrence-free survival after complete surgical resection of local primary gastrointestinal stromal tumors based on deep learning. EBioMedicine, 2019, 39, 272-279.	6.1	32
41	Contrast opacification difference of mural artery and the transluminal attenuation gradient on coronary computed tomography angiography for detection of systolic compression of myocardial bridge. Surgical and Radiologic Anatomy, 2018, 40, 757-767.	1.2	0
42	Radiation Dose Reduction by Using CT with Iterative Model Reconstruction in Patients with Pulmonary Invasive Fungal Infection. Radiology, 2018, 288, 285-292.	7.3	21
43	Use of T <sub>1</sub> relaxation time in rotating frame (T <sub>1</sub> i) and apparent diffusion coefficient to estimate cerebral stroke evolution. Journal of Magnetic Resonance Imaging, 2018, 48, 1247-1254.	3.4	9
44	Connectivityâ€based parcellation of the nucleus accumbens into core and shell portions for stereotactic target localization and alterations in each <scp>NA</scp> c subdivision in m <scp>TLE</scp> patients. Human Brain Mapping, 2018, 39, 1232-1245.	3.6	12
45	Gd-EOB-DTPA-enhanced T1ϕimaging vs diffusion metrics for assessment liver inflammation and early stage fibrosis of nonalcoholic steatohepatitis in rabbits. Magnetic Resonance Imaging, 2018, 48, 34-41.	1.8	18
46	Diagnostic value of six MRI features for central neurocytoma. European Radiology, 2018, 28, 4306-4313.	4.5	9
47	Influence of tube potential on quantitative coronary plaque analyses by low radiation dose computed tomography: a phantom study. International Journal of Cardiovascular Imaging, 2018, 34, 1315-1322.	1.5	4
48	Imaging manifestations of sepsisâ€associated encephalopathy. International Journal of Imaging Systems and Technology, 2018, 28, 196-206.	4.1	0
49	Cortical thickness reductions associate with abnormal resting-state functional connectivity in non-neuropsychiatric systemic lupus erythematosus. Brain Imaging and Behavior, 2018, 12, 674-684.	2.1	18
50	Brain white matter structural networks in patients with non-neuropsychiatric systemic lupus erythematosus. Brain Imaging and Behavior, 2018, 12, 142-155.	2.1	18
51	Glucose functionalized carbon quantum dot containing organic radical for optical/MR dual-modality bioimaging. Materials Science and Engineering C, 2018, 82, 190-196.	7.3	30
52	Detecting GPC3-Expressing Hepatocellular Carcinoma with L5 Peptide-Guided Pretargeting Approach: In Vitro and In Vivo MR Imaging Experiments. Contrast Media and Molecular Imaging, 2018, 2018, 1-11.	0.8	11
53	Radiomics signature of computed tomography imaging for prediction of survival and chemotherapeutic benefits in gastric cancer. EBioMedicine, 2018, 36, 171-182.	6.1	140
54	Preoperative histogram analysis of intravoxel incoherent motion (IVIM) for predicting microvascular invasion in patients with single hepatocellular carcinoma. European Journal of Radiology, 2018, 105, 65-71.	2.6	46

#	Article	IF	CITATIONS
55	A radiomics nomogram for preoperative prediction of microvascular invasion risk in hepatitis B virus-related hepatocellular carcinoma. Diagnostic and Interventional Radiology, 2018, 24, 121-127.	1.5	142
56	Non-invasive monitoring of <i>in vivo</i> hydrogel degradation and cartilage regeneration by multiparametric MR imaging. Theranostics, 2018, 8, 1146-1158.	10.0	75
57	Multifunctional NIR-responsive poly(vinylpyrrolidone)-Cu-Sb-S nanotheranostic agent for photoacoustic imaging and photothermal/photodynamic therapy. Acta Biomaterialia, 2018, 74, 334-343.	8.3	34
58	Use of intravoxel incoherent motion diffusion-weighted MR imaging for assessment of treatment response to invasive fungal infection in the lung. European Radiology, 2017, 27, 212-221.	4.5	14
59	Alterations of white matter structural networks in patients with non-neuropsychiatric systemic lupus erythematosus identified by probabilistic tractography and connectivity-based analyses. NeuroImage: Clinical, 2017, 13, 349-360.	2.7	14
60	Mitochondrial targeted fluorescent probe with AIE characteristics for bioimaging. Materials Science and Engineering C, 2017, 77, 129-135.	7.3	15
61	A novel fluorescence probe based on triphenylamine Schiff base for bioimaging and responding to pH and Fe 3+. Materials Science and Engineering C, 2017, 72, 551-557.	7.3	31
62	Clinical, radiological, pathological and prognostic aspects of intraventricular oligodendroglioma: comparison with central neurocytoma. Journal of Neuro-Oncology, 2017, 135, 57-65.	2.9	4
63	Conjugated Polymer Containing Organic Radical for Optical/MR Dual-Modality Bioimaging. ACS Applied Materials & Interfaces, 2017, 9, 44316-44323.	8.0	18
64	Nonâ€enhanced <scp>MR</scp> lymphography of the thoracic duct: improved visualization following ingestion of a high fat meal–initial experience. Clinical Physiology and Functional Imaging, 2017, 37, 730-733.	1.2	10
65	Gastrin-releasing peptide receptor-targeted gadolinium oxide-based multifunctional nanoparticles for dual magnetic resonance/fluorescent molecular imaging of prostate cancer. International Journal of Nanomedicine, 2017, Volume 12, 6787-6797.	6.7	14
66	Spatial Disassociation of Disrupted Functional Connectivity for the Default Mode Network in Patients with End-Stage Renal Disease. PLoS ONE, 2016, 11, e0161392.	2.5	13
67	Role of intratumoral flow void signs in the differential diagnosis of intracranial solitary fibrous tumors and meningiomas. Journal of Neuroradiology, 2016, 43, 325-330.	1.1	15
68	MRI-based estimation of liver function by intravoxel incoherent motion diffusion-weighted imaging. Magnetic Resonance Imaging, 2016, 34, 1220-1225.	1.8	19
69	Growth patterns of craniopharyngiomas: clinical analysis of 226 patients. Journal of Neurosurgery: Pediatrics, 2016, 17, 418-433.	1.3	51
70	A highly selective and sensitive fluorescent chemosensor for detection of CN <sup>â^'</sup> , SO <sub>3</sub> <sup>2âr'</sup> and Fe <sup>3+</sup> based on aggregation-induced emission. Journal of Materials Chemistry C, 2016, 4, 383-390.	5.5	93
71	Organic Radical Contrast Agents Based on Polyacetylenes Containing 2,2,6,6â€Tetramethylpiperidine 1â€Oxyl (TEMPO): Targeted Magnetic Resonance (MR)/Optical Bimodal Imaging of Folate Receptor Expressing HeLa Tumors in Vitro and in Vivo <sup>a</sup> . Macromolecular Bioscience, 2015, 15, 788-798.	4.1	28
72	Lung MRI of invasive fungal infection at 3 Tesla: evaluation of five different pulse sequences and comparison with multidetector computed tomography (MDCT). European Radiology, 2015, 25, 550-557.	4.5	25

#	Article	IF	CITATIONS
73	Altered brain spontaneous activity and connectivity network in irritable bowel syndrome patients: A resting-state fMRI study. Clinical Neurophysiology, 2015, 126, 1190-1197.	1.5	49
74	Denoising MR Images Using Non-Local Means Filter with Combined Patch and Pixel Similarity. PLoS ONE, 2014, 9, e100240.	2.5	29
75	Optimal region-of-interest MRI R2* measurements for the assessment of hepatic iron content in thalassaemia major. Magnetic Resonance Imaging, 2014, 32, 647-653.	1.8	3
76	Fetus MRI at 7 T: \${B}_{1}\$ Shimming Strategy and SAR Safety Implications. IEEE Transactions on Microwave Theory and Techniques, 2013, 61, 2146-2152.	4.6	13